Biophysical Journal, Volume *111*

Supplemental Information

Effects of Dimethyl Sulfoxide on Surface Water near Phospholipid Bilayers

Yuno Lee, Philip A. Pincus, and Changbong Hyeon

SUPPORTING INFORMATION

Effects of sucrose on surface water. In order to assure that DMSO effect on water as a cryoprotectant is specific, we also studied the effect of another cosolvent, sucrose, on surface water.

First, differences of sucrose from DMSO are clear from the density profiles calculated for water and sucrose. The water density starts to deviate from the bulk value farther away from the solvent-bilayer interface (Fig.S5a), resulting in a greater interface width (greater value of ξ. See Fig.S6a). An increase of the cosovlent concentration changes the interface width in opposite direction as compared to DMSO; ξ increases with the sucrose concentration (X_{sucrose}), whereas it decreases with X_{DMSO} (Fig.S6a). Furthermore, in contrast to DMSO solution, a water rich layer is no longer observed in sucrose solution even at high X_{sucrose} (Fig.S6a), and sucrose molecules accumulates on the bilayer surface (Fig.S5b). Importantly, $\langle \mathcal{Q} \rangle(z)$ indicates that the tetrahedral structure of the water H-bond network (1, 2) is better preserved in sucrose than in DMSO solution (Compare Fig.S5c with Fig.2d, or see Fig.S6b), suggesting that DMSO is a better cryoprotectant.

Next, the local diffusivity profiles of water in the sucrose solution show qualitative difference from those in DMSO solution. In the sucrose solution, both $D_{\mathrm{w}}(z; X_{\mathrm{sucrose}})$ and $D_{\mathrm{w}}(z; X_{\mathrm{sucrose}})/D_{\mathrm{w}}^{\mathrm{bulk}}(X_{\mathrm{sucrose}})$ decrease monotonically from the bulk to bilayer, and the water diffusivity hump is no longer observed (Figs.S5d, e, f). Furthermore, unlike DMSO solutions, the diffusivity profiles $D_{\mathrm{w}}(z; X_{\mathrm{sucrose}})/D_{\mathrm{w}}^{\mathrm{bulk}}(X_{\mathrm{sucrose}})$ collapse onto a single curve in sucrose solution (Fig.S5f). The qualitatively different effects of DMSO and sucrose on the surface water dynamics are highlighted by plotting the surface-to-bulk ratio of water diffusion constant, $q_{\mathrm{sucrose}} \equiv D_{\mathrm{w}}^{\mathrm{surf}}/D_{\mathrm{w}}^{\mathrm{bulk}}$ as a function of X_{sucrose} (Fig.4a) where $D_{\mathrm{w}}^{\mathrm{surf}}$ was calculated at $|z| \approx 22$ Å. While q_{sucrose} does not change with increasing X_{sucrose}, an increase of q_{DMSO} with X_{DMSO} is evident (Fig.4a). This suggests that the surface water dynamics is relatively insensitive to DMSO, while both the surface and bulk water dynamics are equally perturbed by sucrose molecules.

Hydrodynamic radii of DMP^- and TMA^+ in DMSO solution. To corroborate the Schrader *et al.*'s experimental result using pulse field gradient NMR measurement on the hydrodynamic radii of DMP^- and TMA^+ in DMSO solution (3) as well as to check the reliability of the molecular force field (Berger force field) used for phospholipids, we obtain the DMSO-dependent hydrodynamic radii ($r_H = k_B T/6\pi\eta D$) of DMP^- and TMA^+ in the bulk by calculating both diffusion constant D from the mean square displacements and solution viscosity (η) (see Fig.S8 and its caption for details). As shown in Fig.S8d, excellent agreement is found for r_H for DMP^- and TMA^+ between the simulations and PFG NMR measurements. Together with the semi-quantitative agreement between simulation and experiment on the bulk/surface water diffusion constants around Tempo (Fig.6) this result gives credence to our simulation results.

References

[1] Errington, J. R., and P. G. Debenedetti, 2001. Relationship between structural order and the anomalies of liquid water. *Nature* 409:318–321.

[2] Kumar, P., S. V. Buldyrev, and H. E. Stanley, 2009. A tetrahedral entropy for water. *Proc. Natl. Acad. Sci. U. S. A.* 106:22130–22134.

[3] Schrader, A. M., S. H. Donaldson, J. Song, C.-Y. Cheng, D. W. Lee, S. Han, and J. N. Israelachvili, 2015. Correlating steric hydration forces with water dynamics through surface force and diffusion NMR measurements in a lipid–DMSO–H2O system. *Proc. Natl. Acad. Sci. U. S. A.* 112:10708–10713.

[4] Luzar, A., and D. Chandler, 1993. Structure and hydrogen bond dynamics of water - dimethyl sulfoxide mixtures by computer simulations. *J. Chem. Phys.* 98:8160–8173.

[5] Packer, K., and D. Tomlinson, 1971. Nuclear spin relaxation and self-diffusion in the binary system, dimethylsulphoxide (DMSO)+ water. *Transactions of the Faraday Society* 67:1302–1314.

[6] Borin, I. A., and M. S. Skaf, 1999. Molecular association between water and dimethyl sulfoxide in solution: a molecular dynamics simulation study. *J. Chem. Phys.* 110:6412–6420.

[7] Cheng, C.-Y., J. Song, J. Pas, L. H. Meijer, and S. Han, 2015. DMSO induces dehydration near lipid membrane surfaces. *Biophys. J.* 109:330–339.

[8] Price, M. L., D. Ostrovsky, and W. L. Jorgensen, 2001. Gas-phase and liquid-state properties of esters, nitriles, and nitro compounds with the OPLS-AA force field. *J. Comp. Chem.* 22:1340–1352.

[9] MacKerell Jr, A., D. Bashford, M. Bellott, R. Dunbrack Jr, J. Evanseck, M. Field, S. Fischer, J. Gao, H. Guo, S. Ha, et al., 1998. All-Atom Empirical Potential for Molecular Modeling and Dynamics Studies of Proteins. *J. Phys. Chem. B* 102:3586–3616.

[10] Palmer, B. J., 1994. Transverse-current autocorrelation-function calculations of the shear viscosity for molecular liquids. *Phys. Rev. E* 49:359.

Table S1: The area per lipid (APL) and the mean bilayer thickness (d_{PP}) at various DMSO, sucrose mol%.

system	mol%	wt%	Time (μs)	APL/Å^2	d_{PP}/Å
lipid-DMSO-H_2O[a]	0	0	0.4	55.5 ± 1.2	41.7 ± 0.7
	2.9	11.4	0.4	60.5 ± 1.7	39.8 ± 0.7
	6.2	22.3	0.4	61.8 ± 1.5	38.7 ± 0.9
	8.7	29.4	0.4	64.7 ± 1.7	37.7 ± 0.9
	11.3	35.5	0.4	62.8 ± 2.0	38.8 ± 0.9
	16.7	46.5	0.4	63.7 ± 1.3	39.4 ± 0.7
	25.0	59.1	0.4	62.5 ± 2.1	38.0 ± 0.9
	33.3	68.5	0.4	64.2 ± 1.9	38.8 ± 0.7
lipid-sucrose-H_2O[b]	1.5	22.3	1	63.7 ± 2.5	37.7 ± 1.1
	2.8	35.5	1	65.0 ± 3.4	37.1 ± 1.5
	4.4	46.5	1	62.1 ± 1.6	38.3 ± 0.9
lipid-Tempo-DMSO-H_2O[b]	0	0	1	54.8 ± 1.0	42.0 ± 0.7
	1	4.2	1	57.8 ± 1.3	40.6 ± 0.8
	2	8.2	1	59.5 ± 1.3	39.9 ± 0.8
	2.9	11.4	1	61.5 ± 1.6	38.9 ± 0.9
	3.5	13.6	1	60.0 ± 1.3	39.7 ± 0.8
	5	18.7	1	63.1 ± 2.0	38.3 ± 0.9
	6.2	22.3	1	62.3 ± 1.4	38.6 ± 0.8
	7.5	26.0	1	63.9 ± 1.8	37.9 ± 0.9
	8.7	29.4	1	63.0 ± 1.6	38.3 ± 0.8
	11.3	35.5	1	62.8 ± 1.9	38.3 ± 1.0

The analysis was done for the last [a] 0.3 and [b] 0.9 μs. The average positions of phosphorus atom in the upper and lower leaflets were used to calculate the mean thickness of bilayer, d_{PP}.

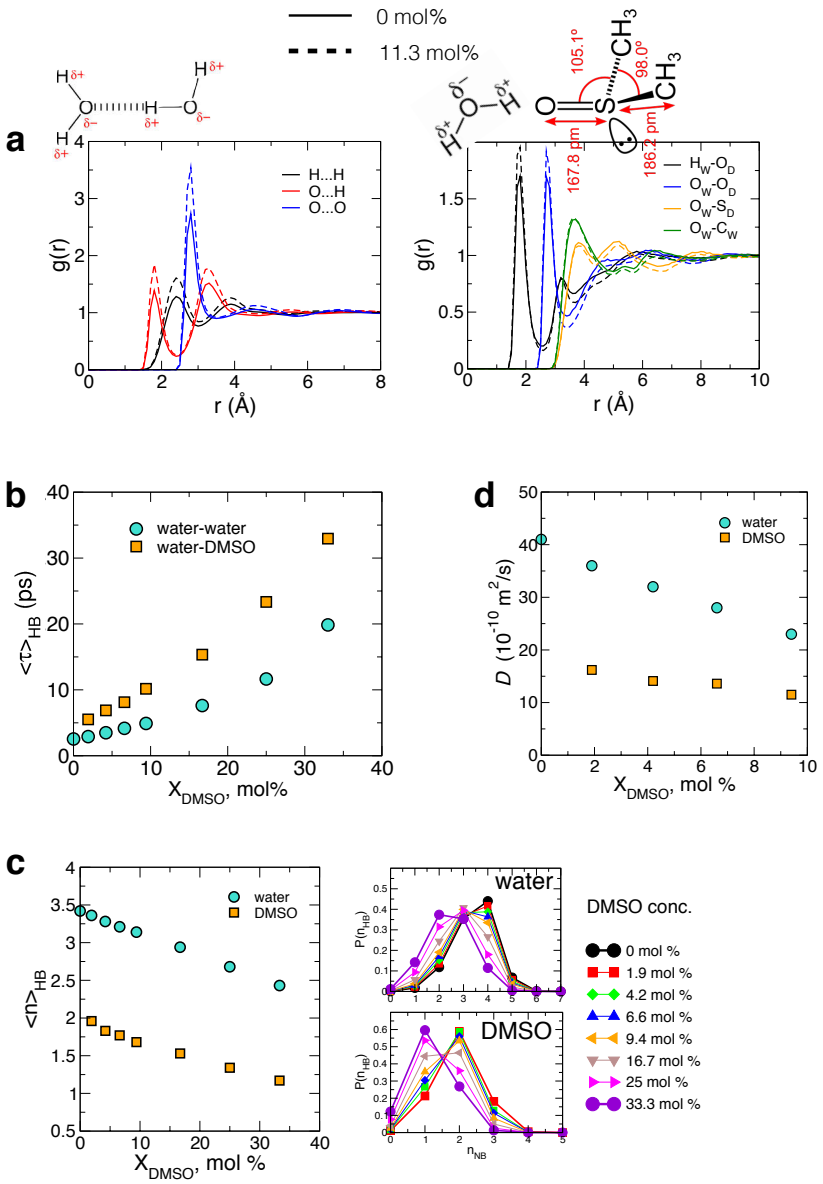

Figure S1: Structural and dynamical characteristics of water and DMSO in varying concentrations of DMSO solution: DMSO, an aprotic cosolvent whose dipole moment (3.96 Debye) is greater than that of water (1.85 Debye), is H-bond acceptor, capable of forming "two" H-bonds with water molecules via sulfonyl group (Fig.S1c), but is not a H-bond donor. The presence of DMSO in aqueous solution increases both the water/water and water/DMSO nearest neighbor correlations (Fig.S1a) and binds more strongly with water than water themselves. Thus, DMSO not only increases the H-bond lifetime (Fig.S1b) but also decreases of the number of H-bonds (Fig.S1c) and diffusion coefficient of both water and DMSO (Fig.S1d), the trend of which continues until the concentration of DMSO reaches 33.3 mol%, at which the 2:1 stoichiometric ratio of water-DMSO is satisfied (4–6). DMSO disrupts the "water structure" beyond the range of nearest molecular neighbors, preventing ice formation at low temperature (4). To recapitulate, DMSO slows down water dynamics and disrupt the tetrahedral ordering of water structure. [(a) Water-water (left) and water-DMSO (right) radial distribution functions at 0 mol% and 11.3 mol% of DMSO solution. DMSO increases inter-molecular correlations. (b) Water-water and water-DMSO H-bond lifetimes as a function of DMSO concentration. (c) Average number of H-bonds ($\langle n_{\mathrm{HB}}\rangle$) around water and DMSO as a function of DMSO concentration (left) and its distribution, $P(n_{\mathrm{HB}})$ for water (top) and DMSO (bottom). (d) Local diffusivity of water and DMSO molecules as a function of DMSO concentration.]

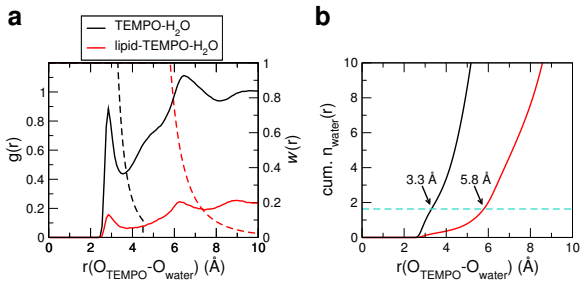

Figure S2: Water radial distribution ($g(r)$) around Tempo in bulk (black) and Tempo in bilayer (red). The initial position-dependent weighting factor $w(r)$ for each case is shown in dashed line (axis label on the right). Cumulative number of water molecules up to r, $n(r) = 4\pi \int_0^r g(r')r'^2 dr'$. For Tempo in bulk, $\sigma_{\text{bulk}} = 3.3$ Å is the position of the 1st solvation shell. For Tempo in bilayer, we chose $\sigma_{\text{bilayer}} = 5.8$ Å, such that the number of waters probed by the Tempo in bilayer for the lifetime calculation is identical to the number of water probed by the Tempo in the bulk, i.e., $n(\sigma_{\text{bulk}}) = n(\sigma_{\text{bilayer}})$.

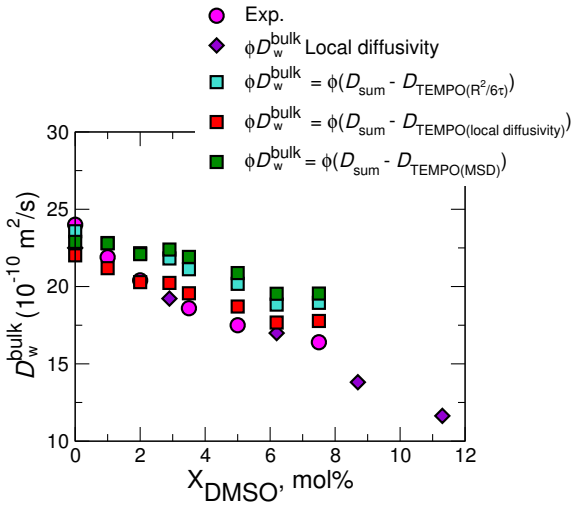

Figure S4: $D_{\text{w}}^{\text{bulk}}$ values using spin-label measurement (7), calculated for pure water, around Tempo moiety in solution. To calculate $D_{\text{w}}^{T,\text{bulk}}$ values around Tempo moiety from simulations, we subtracted the contribution of Tempo from the total diffusion constant. All the four different ways of calculating diffusion constant of bulk water (using Eq.3, Eq.2, mean square displacement) give results comparable to each other.

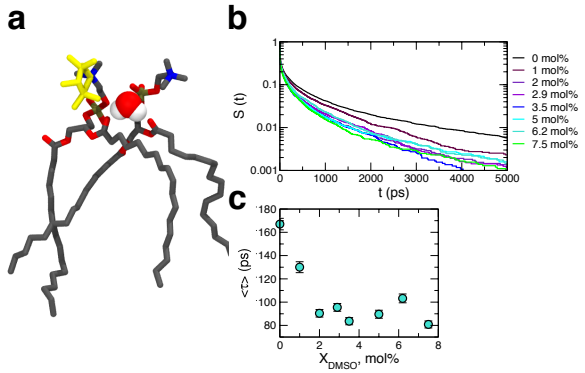

Figure S3: Releasing kinetics of water from Tempo moiety (depicted in yellow). (a) A snapshot of a water molecule trapped between glycerol oxygens at $X_{\text{DMSO}} = 0$ mol%. (b) Survival probability $S(t)$ of water around the nitroxide radical oxygen. (c) The mean escape time ($\langle\tau\rangle$) of water from the nitroxide radical oxygen of Tempo as a function of X_{DMSO}. $\langle\tau\rangle$ is used to estimate the diffusion constant of water around Tempo.

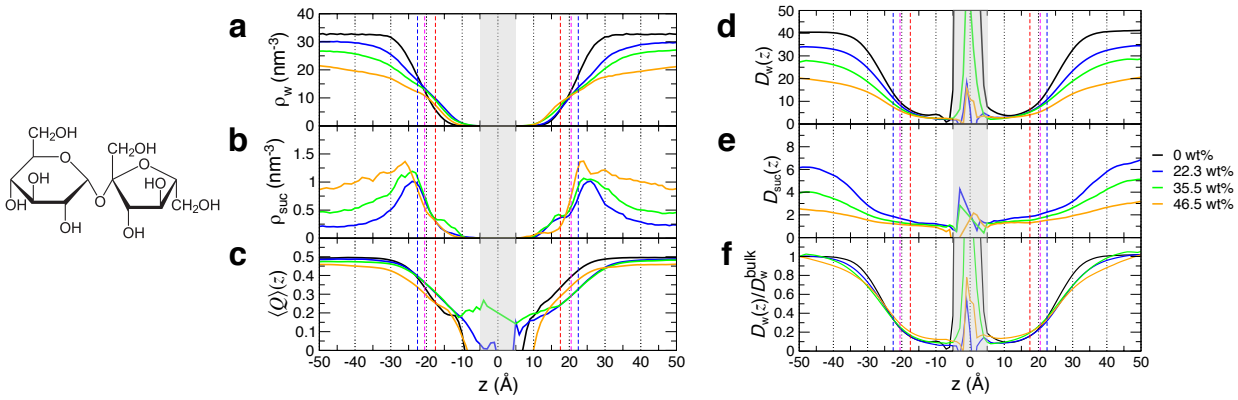

Figure S5: Effects of sucrose on water molecules on bilayer surfaces at various sucrose weight percent $X_{\text{sucrose}} = 0$, 22.3, 35.5, 46.5 wt%. Density profiles of **(a)** water and **(b)** sucrose. **(c)** Tetrahedral order parameter. Local diffusivities ($\times 10^{-10}$ m^2/s) of **(d)** water and **(e)** sucrose. **(f)** Water diffusivity normalized by the bulk diffusion constant.

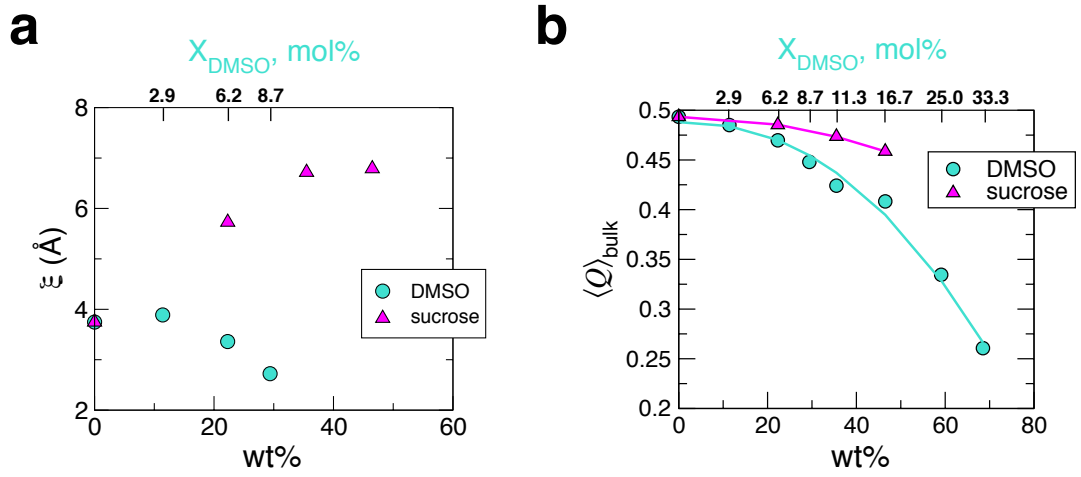

Figure S6: Disparate effects of DMSO and sucrose on water structure and dynamics. (a) The width (2ξ) of solvent-bilayer interface as a function of cosolvent concentration (weight %). Each ξ was obtained by fitting the density profile to Eq.4. (b) Comparison of tetrahedral order parameters probing the water structure at varying weight % of cosolvents (DMSO and sucrose) in the bulk. DMSO is more efficient than sucrose in disrupting the tetrahedral geometry of water H-bond network.

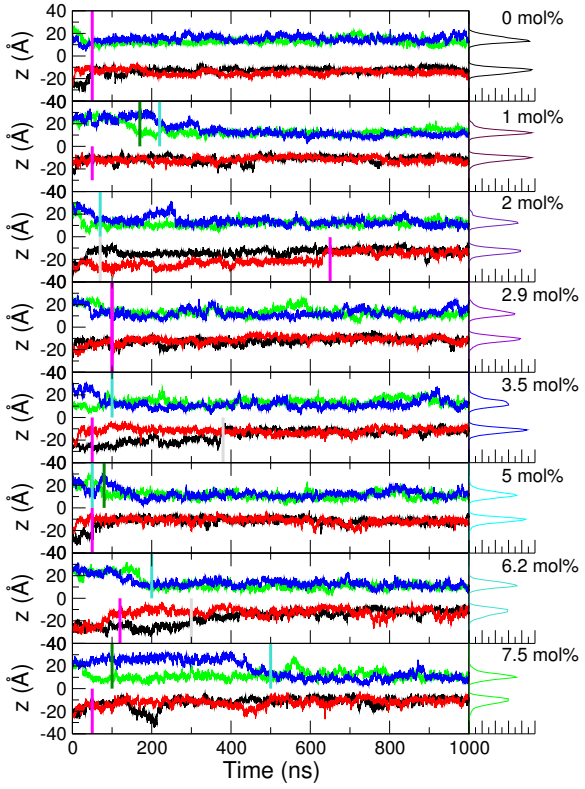

Figure S7: Dynamics of Tempo moiety attached to the head group at various DMSO concentrations are probed using the position of the nitroxide oxygen along the z-axis. Time trajectories obtained from the four Tempo moieties are shown in different colors (blue, green from the upper leaflet, and black, red from the lower leaflet). Note the position of Tempo moiety undergoes large fluctuation over time. Surface water diffusion constants were evaluated using the simulation data collected after the Tempo-PC probe was relaxed from the initial position, reaching the steady state dynamics, which is specified with the bars in each graph. The lifetime analysis of water around Tempo in Fig.S3 was conducted for the time intervals after these bars.

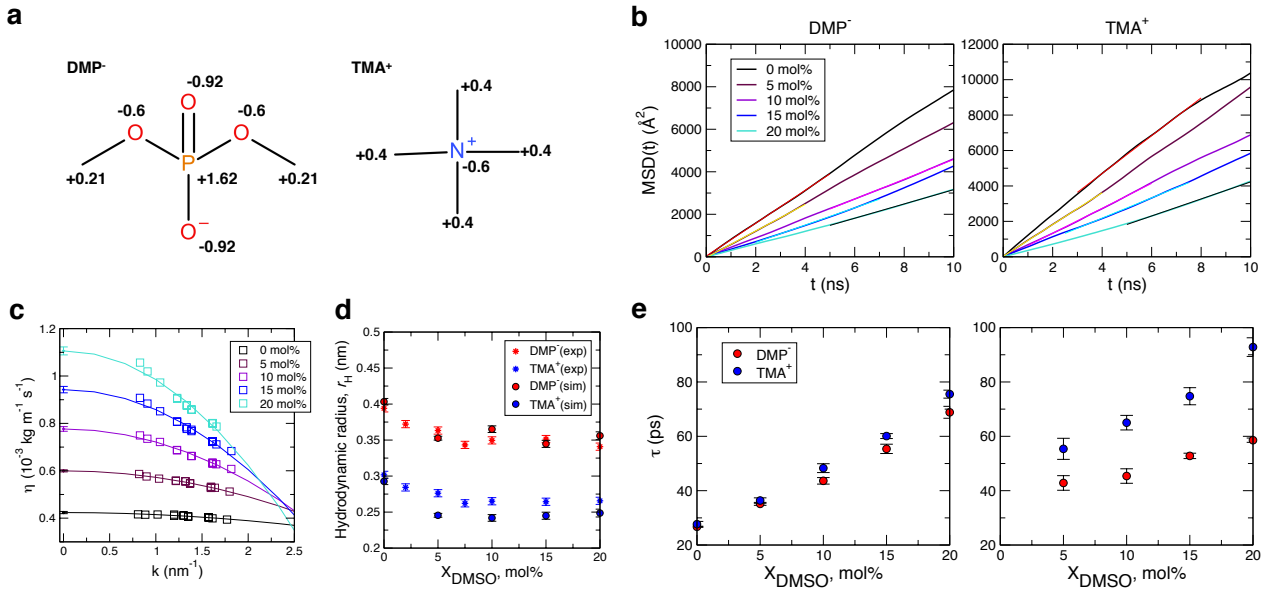

Figure S8: Simulations of PC head groups, dimethyl phosphate (DMP^-) and tetramethylammonium (TMA^+), at various DMSO concentrations (0 – 20 mol%) to estimate their hydrodynamic radii r_H in the bulk. Simulation results using Berger lipid force field essentially reproduce the experimental results of r_H, reported by Schrader *et al.*(3). (a) Chemical structure and partial charges of DMP^- and TMA^+. The force field parameters of DMP^- and TMA^+ except for the partial charges are based on the parameters of Berger lipid force field. The partial charges of DMP^- were taken from OPLS force field (8) that has the closest charge composition with Berger lipid force field. For TMA^+, the charge of nitrogen atom was modified from -0.5 to -0.6 in accord with the standard CHARMM force fields for TMA^+ (9), so as to adjust the net charge to be $+1$. (b) Time-averaged mean square displacement (MSD) of phosphorus atom in DMP^- and nitrogen atom in TMA^+ to calculate diffusion constant of PC head group. The slopes of MSD, depicted as the lines with different colors, were obtained by linear fits. (c) Solvent viscosities of DMSO-H_2O systems were obtained using transverse-current autocorrelation-function (TCAF) calculation (10). Additional DMSO-H_2O mixture systems at various DMSO concentrations were also simulated to predict the solvent viscosity. To obtain the viscosity at infinite wavelength, the k-dependent viscosities are fitted with $\eta(k) = \eta_0(1 - ak^2)$ where η_0 is the infinite system limit of η. The resulting fit and estimated viscosity (η_0) at $k = 0$ is given by solid line and diamond symbol with error bar, respectively. (d) Hydrodynamic radii (r_H) of DMP^- and TMA^+ calculated in the bulk solution with increasing X_{DMSO}. The calculated diffusion (D) and viscosity (η) values were used to compute r_H of the solutes in the DMSO-H_2O mixtures, based on the Stokes-Einstein relation. $D = \frac{k_B T}{6\pi\eta r_H}$, where k_B is Boltzmann's constant and T is the temperature. As a result, the calculated viscosity values are lower and diffusion constants are faster than experimentally obtained values. When the two values are multiplied to yield $r_H = k_B T/6\pi\eta D$, The r_H values, obtained by multiplying the two aforementioned values, are in excellent agreement with the radii acquired from PFG NMR measurements ($*$) (3). (e) X_{DMSO}-dependent lifetimes of water (left) and DMSO (right) in the first solvation shell around DMP^- and TMA^+.